AIP | The Journal of Chemical Physics

The effect of divalent vs. monovalent ions on the swelling of Mucin-like polyelectrolyte gels: Governing equations and equilibrium analysis

S. Sircar, J. P. Keener, and A. L. Fogelson

Citation: J. Chem. Phys. **138**, 014901 (2013); doi: 10.1063/1.4772405
View online: http://dx.doi.org/10.1063/1.4772405
View Table of Contents: http://jcp.aip.org/resource/1/JCPSA6/v138/i1
Published by the American Institute of Physics.

The effect of divalent vs. monovalent ions on the swelling of Mucin-like polyelectrolyte gels: Governing equations and equilibrium analysis

S. Sircar, J. P. Keener, and A. L. Fogelson
Department of Mathematics, University of Utah, Salt Lake City, Utah 84112, USA

(Received 21 June 2012; accepted 30 November 2012; published online 7 January 2013)

We introduce a comprehensive model of a mucin-like polyelectrolyte gel swelling-deswelling which includes the ion-mediated crosslinking of polymer strands and the exchange of divalent and monovalent ions in the gel. The gel is modeled as a multi-phase mixture which accounts for the polymer and solvent volume fractions and velocities as well as ionic species concentrations. Motion is determined by force balances involving viscous, drag, and chemical forces. The chemical forces are derived from a free energy which includes entropic contributions as well as the chemical and electrostatic interactions among the crosslinked polymer, uncrosslinked polymer, and the ionic solvent. The unified derivation produces all the classical effects (van't Hoff osmotic pressure, Donnan equilibrium potential, Nernst-Planck motion of ions) as well as expressions for Flory interaction parameter and the standard free energy parameters that explicitly depend on the gel chemistry and crosslink structure. For this model, we show how the interplay between ionic bath concentrations, ionic binding, and transient divalent crosslinking leads to a variety of swelled and deswelled phases/phase transitions. In particular, we show how the absorption of divalent ions can lead to a massive deswelling of the gel. We conclude that the unique properties of mucin-like gels can be explained by their ionic binding affinities and transient divalent crosslinking. © *2013 American Institute of Physics*. [http://dx.doi.org/10.1063/1.4772405]

I. INTRODUCTION

Mucus is a polyelectrolyte biogel that displays unusual swelling and deswelling characteristics when compared to other polyelectrolyte gels. Mucus plays a critical role as a protective, exchange, and transport medium in the digestive, respiratory, and reproductive systems of humans and other vertebrates.[1,2] Its swelling and deswelling is of special interest because of its role in a variety of diseases including cystic fibrosis.[3–6] Mucin polymers are long-chain, negatively charged glycoproteins whose conformation depends strongly on factors such as pH, ionic strength, and ionic bath composition.[7] Mucin is present in secretory vesicles at very high concentrations where they are shielded primarily by a combination of divalent ions (e.g., Ca^{2+}).[6] Experiments show that the mucus gel may swell explosively, up to 600-fold, in times that are the order of a few seconds, a process not observed in hydrogel swelling.[8,9] Experiments also confirm that this rapid and massive expansion of the mucus gel is driven by an exchange of calcium in the vesicle for sodium in the extracellular environment.[2] Further, experiments demonstrate that the exocytosed mucin can be recondensed if the calcium concentration of the ionic medium is increased sufficiently.[1]

An explanation for this behavior may be found in the difference between the way charges are shielded by divalent ions compared to monovalent ions. A polyelectrolyte gel is negatively charged and all charges must be balanced by counterions. There are several possible counterions, including sodium, calcium, potassium, and hydrogen. The important difference between these is that calcium is divalent and so it must balance two negative charges rather than one. Hence, a divalent Ca^{2+} ion can act as a "crosslinker" between two polymer strands, allowing much tighter condensation than when the negative charges of the network are shielded by monovalent ions. However, these divalent crosslinking "bonds" (i.e., affinities) are much weaker than covalent bonds hence are not permanent, explaining the ability of these gels to expand so rapidly. The transient nature of this crosslinking is corroborated by experimental and simulation findings showing that divalent ions do not form stable crosslinks between anionic polyelectrolyte chains.[10–14] In any process in which there is an exchange of divalent ions for monovalent ions, the crosslinking structure of the polymer network must change, thereby modifying the amount of condensation or hydration. If this is the controlling mechanism, it also follows that changes in the ionic affinity of the gel or changes in the ionic concentrations of the bath in which the gel is immersed affect the hydration state.[8]

The purpose of this paper is to give a careful and complete derivation of a model describing the kinetics of polyelectrolyte mucin-like gels, and to use this model to show how the behavior of a polyelectrolyte gel in a divalent ionic environment differs from that of the same gel in a monovalent ionic environment. The model we develop explicitly accounts for the difference between shielding by monovalent ions and transient crosslinking by divalent ions and for the monovalent/divalent concentration of the bath environment. With this model we can determine how the mixture of monovalent and divalent ions in a chemical bath surrounding a gel affects the gel's equilibria.

Previous work on polyelectrolyte gels builds on the classic work of Tanaka on hydrogels,[15] and includes effects of osmotic pressure arising from the charge-induced Donnan equilibrium,[16,17] the Poisson-Boltzmann equation and Biot's theory of poroelasticity,[18] as well as phenomenological modifications of Flory-Higgins theory to capture some effects of multi-ionic cations.[19,20] Furthermore, in previous gel swelling literature, the Flory interaction parameter was either chosen to be a function of temperature alone or of temperature and polymer volume fraction.[17,21]

In Sec. II of this paper, we provide the details of the model including derivation of multi-phase transport equations, the interface conditions, the reaction-advection equations which take into account the ionic activity of polyelectrolyte gels in a chemical medium, and the chemical potentials which account for the long-range (electrostatic) and the short-range (nearest neighbor) polymer-solvent interactions on a lattice. To our knowledge, we provide here the first systematic derivation of the equations of motion for a multi-species polyelectrolyte gel (with solvent, polymer and multiple ion types), that includes all the classical effects (van't Hoff osmotic pressure, Donnan equilibrium potential, Nernst-Planck motion of ions) as well as the Flory interaction parameter and the standard free energies which incorporate the effects of the underlying chemistry and gel structure. In Sec. III, we study the equilibria of the model giving a thorough analysis of these for different ionic binding affinities, interaction energies and ionic bath concentrations. We show how these parameters control the swelling/deswelling characteristics of the gel and lead to interesting phases and phase transition behavior.

II. MODEL DESCRIPTION

We view a polymer gel as a multi-component material, consisting of k different types of particles. Specifically, we have solvent particles, polymers, and several small molecular ion species. The polymer is assumed to be made up of monomers (i.e., charge units), denoted as M, with volume ν_m, each of which carries a single negative charge. In addition, there are ions, both positively and negatively charged, which are dissolved in the solvent. To be specific, we identify the positive ions as hydrogen, sodium, and calcium, but it is an easy generalization to include additional ions. The negatively charged ions could include hydronium, chloride, and others. However, because the negatively charged ions are assumed to be not involved in any binding reactions with mucus, acting only as counterions to positive charges, we identify these ions by the name chloride. Positively charged ions can bind to the negatively charged monomers via the reactions

$$\begin{aligned} &\mathrm{M}^- + \mathrm{H}^+ \rightleftharpoons \mathrm{HM}, \mathrm{M}^- + \mathrm{Na}^+ \rightleftharpoons \mathrm{NaM}, \\ &\mathrm{M}^- + \mathrm{Ca}^{++} \rightleftharpoons \mathrm{MCa}^+, \mathrm{M}^- + \mathrm{MCa}^+ \rightleftharpoons \mathrm{M_2Ca}. \end{aligned} \tag{1}$$

With these reactions it is assumed that all the binding sites/charge sites are identical and the binding affinities for the different ions may be different. In reality, there could be different kinds of binding sites for each ion with different binding affinities. The species $\mathrm{M_2Ca}$ are crosslinked monomer pairs, and the species M^-, MCa^+, NaM, and HM are different monomer species, all of which move with the polymer velocity. The ion species Ca^{2+}, Na^+, H^+, and Cl^- are freely diffusible, but because they are ions, their movement is restricted by the requirement to maintain electroneutrality. Finally, because a small amount of water dissociates into hydrogen and hydronium, we are guaranteed that there are always some positive and negative ions in the solvent.

A. Equations of motion and interface conditions

In this section we use the minimum rate of work principle (also known as the Helmholtz minimum energy dissipation rate principle[22,23]) to derive equations of motion and interface conditions for the multi-phase fluid comprised of particles of different sizes. (A similar approach was used in Ref. 24 to derive two-phase equations for the motion of swimming bacteria.) Suppose we have some volume V of a mixture comprised of k types of particles each with particle density (number of particles per unit volume) n_j, and particle volumes $\nu_j, j = 1, \ldots, k$. Specifically, we have a polymer network with monomeric particle density $n_1 = n_m$, solvent, with particle densities $n_2 = n_s$, and other molecular species with particle density n_j, $j = 3, \ldots, k$. For each of these components there is a velocity, $\mathbf{v}_j$, the polymer network velocity $\mathbf{v}_1 = \mathbf{v}_p$, the solvent velocity $\mathbf{v}_2 = \mathbf{v}_s$ and molecular species velocities $\mathbf{v}_j$, $j = 3, \ldots, k$. Conservation of particles implies that

$$\frac{\partial n_j}{\partial t} + \nabla \cdot (\mathbf{v}_j n_j) = \sum_i (R_{i,j} - R_{j,i}), \tag{2}$$

where $R_{i,j}$ represents the rate of conversion of particle type i into particle type j. We assume that chemical reactions do not change the number density of solvent or monomer species, so that $R_{i,j} = 0$ if either i or j is 1 or 2. The volume fractions for solvent and polymer are $\theta_s = \nu_s n_s$ and $\theta_p = \nu_m n_p$, and θ_p satisfies

$$\frac{\partial \theta_p}{\partial t} + \nabla \cdot (\mathbf{v}_p \theta_p) = 0. \tag{3}$$

We assume that the other molecular species do not contribute significantly to the volume (i.e., we take $\nu_j = 0, j = 3, \ldots, k$). Therefore, $\theta_p + \theta_s = 1$, so it follows from (2) that

$$\nabla \cdot (\theta_s \mathbf{v}_s + \theta_p \mathbf{v}_p) = 0. \tag{4}$$

For this mixture the total rate of work is

$$\begin{aligned} D_E = \int_\Omega \Bigg(&\frac{1}{2} n_m \nu_m \sigma_p(\mathbf{v}_p) : \dot{\varepsilon}(\mathbf{v}_p) + \frac{1}{2} n_s \nu_s \sigma_s(\mathbf{v}_s) : \dot{\varepsilon}(\mathbf{v}_s) \\ &+ \frac{1}{2} \xi \frac{n_m n_s}{n_m + n_s} (\mathbf{v}_p - \mathbf{v}_s)^2 \\ &+ \frac{1}{2} \sum_{j \geq 3} \xi_j \frac{n_j n_s}{n_j + n_s} (\mathbf{v}_s - \mathbf{v}_j)^2 - \sum_j \mu_j \nabla \cdot (n_j \mathbf{v}_j) \Bigg) dV. \end{aligned} \tag{5}$$

Here $\dot{\varepsilon}(\mathbf{v}) = \frac{1}{2}(\nabla \mathbf{v} + \nabla \mathbf{v}^T)$ is the rate of strain tensor, $\sigma_j(\mathbf{v}) = \eta_j \dot{\varepsilon}(\mathbf{v}) + \lambda_j I \nabla \cdot \mathbf{v}$ is the stress tensor, where $\eta_j > 0$ and λ_j, $j = p, s$, are the viscosities. Thus, the first two terms in D_E represent the rate of energy dissipated by viscosity within

the polymer and solvent. The third term represents the energy dissipation rate due to drag between solvent and polymer, and is proportional to the total number of interactions between the two particle types. The fourth term is the rate of work due to drag between solvent and ion species particles. The fifth term corresponds to the rate of work required to change the number density of particle j against its chemical potential μ_j. Expressions for the chemical potentials are derived in Sec. II B. In this expression, we have ignored self interaction (viscosity) of the ions, drag between the different ion species and drag between each ion species and monomer under the assumption that the ion species are dissolved in the solvent.

According to the minimum rate of work principle, the velocities are those which minimize the rate of work D_E. Accordingly, we seek to minimize the functional D_E over all admissible functions $(\mathbf{v}_j, P, \Psi_e)$, $j = 1, 2, \ldots, k$. Here, P, the pressure, and Ψ_e, the electrical potential, are Lagrange multipliers used to enforce the incompressibility condition (4), and electroneutrality, and they appear in the chemical potentials, as described below.

Following standard variational arguments (summarized in the Appendix), and assuming the ionic molecular species are dilute, we find that the equations of motion are the force balance equations

$$\nabla \cdot (\theta_p \sigma_p(\mathbf{v}_p)) - \xi \frac{\theta_p}{\nu_m} \phi_s (\mathbf{v}_p - \mathbf{v}_s) - \frac{\theta_p}{\nu_m} \nabla \mu_p = 0 \tag{6}$$

and

$$\nabla \cdot (\theta_s \sigma_s(\mathbf{v}_s)) - \xi \frac{\theta_s}{\nu_s} \phi_p (\mathbf{v}_s - \mathbf{v}_p) - \frac{\theta_s}{\nu_s} \sum_{j \geq 3} \xi_j \hat{\phi}_j (\mathbf{v}_s - \mathbf{v}_j) - \frac{\theta_s}{\nu_s} \nabla \mu_s = 0, \tag{7}$$

where $\phi_s = \frac{n_s}{n_m + n_s}$, $\phi_p = \frac{n_p}{n_m + n_s}$, $\hat{\phi}_j = \frac{n_j}{\sum_{i \neq 1} n_i}$ for $j \geq 3$, are the polymer, solvent, and ion species per total solvent particle fractions, respectively, while the ion species satisfy the force balance equation,

$$\xi_j n_j (\mathbf{v}_s - \mathbf{v}_j) - n_j \nabla \mu_j = 0, \quad j \geq 3. \tag{8}$$

The first two of these equations are analogous to the Stokes equation for a Newtonian fluid. Note that one can use (8) to eliminate the ion velocities from (7) yielding

$$\nabla \cdot (\theta_s \sigma_s(\mathbf{v}_s)) - \xi \frac{\theta_s}{\nu_s} \phi_p (\mathbf{v}_s - \mathbf{v}_p) - \frac{\theta_s}{\nu_s} \sum_{j \geq 3} \hat{\phi}_j \nabla \mu_j - \frac{\theta_s}{\nu_s} \nabla \mu_s = 0, \tag{9}$$

demonstrating that the solvent "feels" forces from the ion chemical potentials. As shown below (39), these include electric as well as entropic forces.

In addition, if there is an edge to the gel, on one side of which (inside the gel) $\theta_p = \theta_p^-$, and on the other side of which (outside the gel) $\theta_p^+ = 0$, $\theta_s^+ = 1$, there are interface conditions,

$$\sigma_p(\mathbf{v}_p^-)\mathbf{n} = \frac{\mu_p^-}{\nu_m}\mathbf{n} \tag{10}$$

for the polymer,

$$(\sigma_s(\mathbf{v}_s^+) - \sigma_s(\mathbf{v}_s^-))\mathbf{n} = \frac{1}{\nu_s}(\mu_s^+ - \mu_s^-)\mathbf{n} \tag{11}$$

for the solvent, and

$$\mu_j^+ = \mu_j^- \tag{12}$$

for the ion species, $j \geq 3$.

B. Chemical potentials

We now determine the free energy and chemical potentials for this material. As above, we suppose there are k different kinds of particles, with particle volumes ν_i, and particle numbers (not number densities) N_i, $i = 1, \ldots, k$. To calculate the chemical potentials, we use the Gibb's free energy

$$G = -k_B T S + U + PV, \tag{13}$$

where U is internal energy, S is entropy, T is temperature, k_B is Boltzmann's constant, P is pressure, and $V = \sum_j \nu_j N_j$ is the total volume of the system. However, we assume that the volume occupied by species $j = 3, \ldots, k$ (which are the ions dissolved in the solvent) is small compared to that of the monomer plus solvent volumes $\nu_m N_n + \nu_s N_s$ and so take $V = \nu_m N_m + \nu_s N_s$. As usual, the chemical potential μ_j is defined as the change in free energy resulting from the addition of a particle of type j, keeping the numbers of all other particles fixed, i.e.,

$$\mu_j = \frac{\partial G}{\partial N_j} = -k_B T \frac{\partial S}{\partial N_j} + \frac{\partial U}{\partial N_j} + \nu_j P, \tag{14}$$

which is the sum of the entropic contribution, μ_j^S, and the contributions due to internal energy and pressure, respectively.

1. Entropic contributions to chemical potentials

The entropy of the system is defined as

$$S = \sum N_i \omega_i, \tag{15}$$

where ω_i is the entropy per particle for the ith particle. Using standard counting arguments (as in Ref. 25), for single-molecule species,

$$\omega_j = -\ln(\hat{\phi}_j), \tag{16}$$

and for polymers consisting of chains of N monomers,

$$\omega_p = -\frac{1}{N} \ln(\hat{\phi}_p), \tag{17}$$

where $\hat{\phi}_p = \frac{N_m}{\sum_i N_i}$ is the monomeric particle fraction, and $\hat{\phi}_s = \frac{N_s}{\sum_i N_i}$ is the solvent particle fraction. Further, we assume that the ion species are dissolved in the solvent only, with polymer volume excluded so that $\hat{\phi}_j = \frac{N_j}{\sum_{i \neq 1} N_i}$ for $j \geq 3$, is ion species per total solvent particle fraction. Since crosslinks are transient, constantly being formed and broken by the binding and unbinding of divalent ions, their effect on the polymeric entropy is different from entropic rubber elasticity, where crosslinking bonds are permanent (i.e., covalent bonds). As

a consequence, we do not include a term in the entropy corresponding to entropic rubber elasticity.

Now we make an approximation. We assume that

$$\frac{\sum_{j\geq 3} N_j}{N_s + N_m} \ll 1, \tag{18}$$

so that $\hat{\phi}_j \approx \phi_j = \frac{N_j}{N_m+N_s}$ for $j = p, s$. With these assumptions, and using that $\mu_j^S = k_B T \frac{\partial(N_j \omega_j)}{\partial N_j}$, we find that

$$\frac{\mu_p^S}{k_B T} = \frac{1}{N} \ln \phi_p - \left(1 - \frac{1}{N}\right) \phi_s, \tag{19}$$

$$\frac{\mu_s^S}{k_B T} = \ln \phi_s - \frac{1}{N} \phi_p + 1 - \phi_s - \sum_{i\geq 3} \hat{\phi}_i, \tag{20}$$

$$\frac{\mu_j^S}{k_B T} = \ln \hat{\phi}_j + 1 - \sum_{i\geq 3} \hat{\phi}_i, \quad j \geq 3. \tag{21}$$

Observe that in the dilute ionic-solution limit, for $j \geq 3$,

$$\hat{\phi}_j = \phi_j (1 - \sigma_I) + O\left(\sigma_I^2\right), \tag{22}$$

where $\sigma_I = \sum_{j\geq 3} \frac{N_j}{N_s} = \sum_{j\geq 3} \phi_j$, $\phi_j = \frac{N_j}{N_s}$. So,

$$\frac{\mu_s^S}{k_B T} = \ln \phi_s + \left(1 - \frac{1}{N}\right) \phi_p - \sigma_I \tag{23}$$

and

$$\frac{\mu_j^S}{k_B T} = \ln \phi_j + 1 - 2\sigma_I, \tag{24}$$

for $j \geq 3$, to leading order in σ_I. The term σ_I in the solvent chemical pressure (23) is the total ion particle fraction and represents osmotic pressure as characterized by van't Hoff's law.

2. Internal energy contribution to chemical potentials

We assume that the internal energy consists of two contributions, long range electrostatic interactions, and short range (nearest neighbor) interactions. The long range electrostatic interactions have energy

$$U_e = \sum_j z_j N_j \Phi_e, \tag{25}$$

where z_i is the charge on the ith ionic species ($z_1 \equiv z_m$ is the average charge per monomer), and Φ_e is the electric potential. For the ion species, we assume there are no additional interactions.

To calculate the short range interaction energy for the polymer and solvent, we note that there are N_m monomers and N_s solvent molecules, for a total of $N_T = N_m + N_s$ particles, and for simplicity assume that they each have z interaction sites (called the coordination number). Of the N_m monomers, αN_m of them are in crosslinked pairs, where α is the crosslink fraction. The other $(1 - \alpha)N_m$ may have a variety of binding or ionized states, but since these states are assumed to affect only long-range interactions, we do not distinguish them. Since the crosslinked particles are connected, for the purposes of this calculation we treat them as a single species. The different species with their pairwise interactions are shown in Fig. 1. The crosslinked particle pairs have $2z$-6, $2z$-4, or $2z$-5 free interaction sites, depending on whether the monomers in the crosslinked pair are both in the middle of a polymer chain, both at the end of a chain, or have one monomer in the middle and the other at the end of a polymer chain, respectively (Figs. 1(a)–1(c)). An uncrosslinked monomer has either z-2 or z-1 free interaction sites, based on its position in the polymer chain (Figs. 1(d) and 1(e)), while the solvent particles have z free interaction sites (Fig. 1(f)).

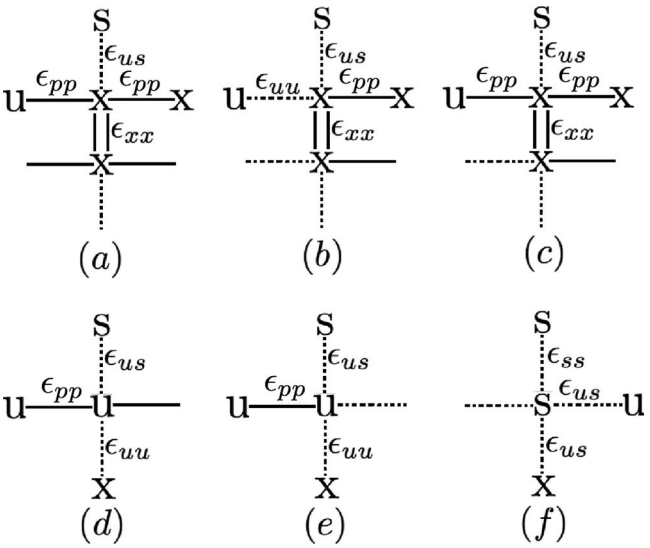

FIG. 1. Pairwise interactions of the different species and their associated interaction energies for: (a)–(c) crosslinked monomers, x, (d) and (e) uncrosslinked monomers, u, and (f) solvent, s. Double solid lines denote crosslinking, single solid lines denote interactions within a polymer chain while the other types of interactions are denoted by dashed lines.

We let $k_B T_0 \epsilon_{xx}$, $k_B T_0 \epsilon_{uu}$, $k_B T_0 \epsilon_{pp}$, $k_B T_0 \epsilon_{us}$, and $k_B T_0 \epsilon_{ss}$ be the interaction energies associated with each crosslinked monomer-monomer interaction, uncrosslinked monomer-monomer interaction, monomer-monomer interaction within a polymer strand, monomer-solvent interaction and solvent-solvent interaction, respectively. T_0 is a reference temperature. The interaction energies for crosslinked, uncrosslinked polymer particles, and solvent particles are

$$F_x^1 = \frac{\alpha}{2} N_m k_B T_0 \left(\frac{N-2}{N}\right)^2 (2\epsilon_{xx} + (2z-6)E_{us} + 4\epsilon_{pp}), \tag{26}$$

$$F_x^2 = \frac{\alpha}{2} N_m k_B T_0 \left(\frac{2}{N}\right)^2 (2\epsilon_{xx} + (2z-4)E_{us} + 2\epsilon_{pp}), \tag{27}$$

$$F_x^3 = \alpha N_m k_B T_0 \frac{2}{N} \frac{N-2}{N} (2\epsilon_{xx} + (2z-5)E_{us} + 3\epsilon_{pp}), \tag{28}$$

$$F_u^1 = (1-\alpha) \frac{N-2}{N} N_m k_B T_0 ((z-2)E_{us} + 2\epsilon_{pp}), \tag{29}$$

$$F_u^2 = (1-\alpha) \frac{2}{N} N_m k_B T_0 ((z-1)E_{us} + \epsilon_{pp}), \tag{30}$$

$$F_s = z N_s k_B T_0 \left(\epsilon_{us} \frac{N_m}{N_T} + \epsilon_{ss} \frac{N_s}{N_T}\right), \tag{31}$$

respectively, where $E_{us} = \epsilon_{uu}\frac{N_m}{N_T} + \epsilon_{us}\frac{N_s}{N_T}$. Each of these is calculated using standard mean-field arguments. For example, for F_u^2 (see Fig. 1(e)), there are $(1-\alpha)N_m$ uncrosslinked monomers, of which $\frac{2}{N}$ are at the ends of a polymer chain. For each of these, one interaction is monomer-monomer, and the remaining $z-1$ interactions are distributed to monomer-monomer, with probability $\frac{N_m}{N_T}$ and monomer-solvent, with probability $\frac{N_s}{N_T}$.

It follows that the total per particle interaction energy is

$$U^I = \frac{1}{2}\frac{1}{N_m+N_s}\left(F_x^1 + F_x^2 + F_x^3 + F_u^1 + F_u^2 + F_s\right) = k_B T_0\left[\frac{i}{2}\phi_p\phi_s + \mu_0^s\phi_s + \mu_0^p\phi_p + \frac{z}{2}\epsilon_{us}\right], \quad (32)$$

where

$$i = z(\epsilon_1+\epsilon_2) - 2\left(1-\frac{1}{N}\right)\epsilon_1 - \epsilon_1\alpha, \quad (33)$$

$$\mu_0^p = -\epsilon_1\frac{z}{2} + \epsilon_4\left(1-\frac{1}{N}\right) + \frac{1}{2}\epsilon_3\alpha, \quad \mu_0^s = -\epsilon_2\frac{z}{2}, \quad (34)$$

and

$$\epsilon_1 = \epsilon_{us} - \epsilon_{uu}, \quad \epsilon_2 = \epsilon_{us} - \epsilon_{ss}, \quad \epsilon_3 = \epsilon_{xx} - \epsilon_{uu}, \quad \epsilon_4 = \epsilon_{pp} - \epsilon_{uu}. \quad (35)$$

(The factor $\frac{1}{2}$ multiplying the sum of energies is to correct for double counting.) The dependences of the interaction parameter i and standard free energies μ_0^p, μ_0^s on α determine the relation between the free energy of the gel and the fraction of polymers crosslinked by divalent ions. Furthermore, the corresponding contributions to chemical potentials are

$$\mu_p^I = k_B T_0\left(\frac{i}{2}\phi_s^2 + \mu_p^0\right), \quad (36)$$

$$\mu_s^I = k_B T_0\left(\frac{i}{2}\phi_p^2 + \mu_s^0\right). \quad (37)$$

Notice that when $\alpha = 0$, U^I in Eq. (32) reduces to the interaction energy found in standard Flory-Huggins theory.[26,27]

In summary, the chemical potential for each species is comprised of four terms

$$\mu_j = k_B T\mu_j^S + \mu_j^I + z_j\Phi_e + \nu_j P. \quad (38)$$

For the ion species, $\mu_j^I = 0$, and we ignore its volume, ν_j, so that

$$\frac{\mu_j}{k_B T} = \ln\phi_j + 1 - 2\sigma_I + z_j\Psi_e, \quad j \geq 3, \quad (39)$$

where $\Psi_e = \frac{\Phi_e}{k_B T}$. Because it is small compared to $\ln\phi_j$, we ignore the term $2\sigma_I$ as well. The polymer and solvent chemical potentials are

$$\frac{\mu_p}{k_B T} = M_p + z_m\Psi_e + \nu_m\frac{P}{k_B T}, \quad (40)$$

$$\frac{\mu_s}{k_B T} = M_s - \sigma_I + \nu_s\frac{P}{k_B T}, \quad (41)$$

where

$$M_p = \left(\frac{1}{N}-1\right)\phi_s + \frac{1}{N}\ln\phi_p + \frac{\mu_p^I}{k_B T}, \quad (42)$$

$$M_s = \left(1-\frac{1}{N}\right)\phi_p + \ln\phi_s + \frac{\mu_s^I}{k_B T}. \quad (43)$$

Finally, the gel-sol interface conditions, Eqs. (10) and (11), become

$$\sigma_p(\mathbf{v}_p^-)\mathbf{n} = \frac{k_B T}{\nu_m}\left(M_p^- + z_m\Psi_e + \nu_m\frac{P}{k_B T}\right)\mathbf{n} \quad (44)$$

and

$$\left(\sigma_s(\mathbf{v}_s^+) - \sigma_s(\mathbf{v}_s^-)\right)\mathbf{n} = \frac{k_B T}{\nu_s}\left(M_s^+ - M_s^- - \sigma_I^+ + \sigma_I^- - \nu_s\frac{P}{k_B T}\right)\mathbf{n}, \quad (45)$$

where $P \equiv P^-$, $P^+ = 0$ and $\Psi_e^- \equiv \Psi_e$, $\Psi_e^+ = 0$. Eliminating P from these we find the single interface condition

$$(\sigma_p(\mathbf{v}_p^-) - \sigma_s(\mathbf{v}_s^-) + \sigma_s(\mathbf{v}_s^+))\mathbf{n} = \Sigma_{net}\mathbf{n}, \quad (46)$$

where Σ_{net} is the net swelling pressure,

$$\frac{\Sigma_{net}}{k_B T} = \frac{M_p^-}{\nu_m} - \frac{M_s^-}{\nu_s} + \frac{T_0}{T}\frac{\mu_s^0}{\nu_s} + \frac{z_m}{\nu_m}\Psi_e + \frac{\sigma_I^-}{\nu_s} - \frac{\sigma_I^+}{\nu_s}. \quad (47)$$

It is worth noting that

$$k_b T\left(\frac{M_p}{\nu_m} - \frac{M_s}{\nu_s}\right) = \frac{d}{d\theta_p}\left(\frac{F_0}{\nu_m N_m + \nu_s N_s}\right), \quad (48)$$

where

$$F_0 = k_B T\left(N_s\ln(\phi_s) + \frac{1}{N}N_m\ln(\phi_p) + (N_m+N_s)U^I\right) \quad (49)$$

is the free energy associated with the polymer-solvent system free of ions.

C. Ionization chemistry

To track the chemical species, we must know how they move and react. The concentrations per total volume of the polymer species are denoted by $x = [M_2Ca]$, $m = [M^-]$, $v = [NaM]$, $w = [MCa^+]$, and $y = [HM]$, with the total monomer concentration,

$$m_T = m + 2x + w + v + y. \quad (50)$$

The concentrations per solvent volume of the ion species are denoted as $c = [Ca^{++}]$, $n = [Na^+]$, $h = [H^+]$, and $c_l = [Cl^-]$. With concentrations expressed in units of moles per liter, the relationship between ion particle fractions ϕ_j and concentrations c_j is $\phi_j = \nu_s N_A c_j$, where N_A is Avagadro's number.

To describe the chemical reactions, we use the law of mass action. Since all the monomer species are advected with the polymer velocity $\mathbf{v}_p$, the monomer species evolve according to

$$\frac{\partial w}{\partial t} + \nabla\cdot\mathbf{v}_p w = k_c m c\theta_s - k_{-c}\phi_s^2 w + k_{-x}\phi_s^2 x - k_x m w, \quad (51)$$

$$\frac{\partial x}{\partial t} + \nabla \cdot \mathbf{v}_p x = k_x m w - k_{-x}\phi_s^2 x, \tag{52}$$

$$\frac{\partial v}{\partial t} + \nabla \cdot \mathbf{v}_p v = k_n m n \theta_s - k_{-n}\phi_s^2 v, \tag{53}$$

$$\frac{\partial y}{\partial t} + \nabla \cdot \mathbf{v}_p y = k_h m h \theta_s - k_{-h}\phi_s^2 y, \tag{54}$$

where $\theta_p = \nu_m N_A m_T$ satisfies Eq. (3), and m is obtained from Eq. (50). Because the unbinding (dissociation) reactions are ionization reactions that require two "units" of solvent, we take the unbinding reaction rates to be $k_{-C}\phi_s^2$, $C = c$, x, n, h, and because calcium is a divalent ion, $2k_x = k_c$ and $k_{-x} = 2k_{-c}$.

It follows from (8) and (39) that the (per solvent volume) flux of the ion species is the classical Nernst-Planck flux

$$J_C = C\left(\mathbf{v}_s - \frac{1}{\xi_C}\nabla\mu_C\right) = C\mathbf{v}_s - \frac{k_B T}{\xi_C}(\nabla C + z_C C \nabla\Psi_e), \tag{55}$$

$$C = c, n, h, c_l,$$

ignoring terms of order ϕ_C^2. It follows that

$$\frac{\partial c}{\partial t} + \nabla\cdot(c\mathbf{v}_s) - \frac{1}{\theta_s}\nabla\cdot\left(\theta_s\frac{k_B T}{\xi_c}(\nabla c + 2c\nabla\Psi_e)\right) = -k_c m c + k_{-c}\frac{\phi_s^2}{\theta_s}w, \tag{56}$$

$$\frac{\partial n}{\partial t} + \nabla\cdot(n\mathbf{v}_s) - \frac{1}{\theta_s}\nabla\cdot\left(\theta_s\frac{k_B T}{\xi_n}(\nabla n + n\nabla\Psi_e)\right) = -k_n m n + k_{-n}\frac{\phi_s^2}{\theta_s}v, \tag{57}$$

$$\frac{\partial h}{\partial t} + \nabla\cdot(h\mathbf{v}_s) - \frac{1}{\theta_s}\nabla\cdot\left(\theta_s\frac{k_B T}{\xi_h}(\nabla h + h\nabla\Psi_e)\right) = -k_h m h + k_{-h}\frac{\phi_s^2}{\theta_s}y, \tag{58}$$

$$\frac{\partial c_l}{\partial t} + \nabla\cdot(c_l\mathbf{v}_s) - \frac{1}{\theta_s}\nabla\cdot\left(\theta_s\frac{k_B T}{\xi_{c_l}}(\nabla c_l - c_l\nabla\Psi_e)\right) = 0, \tag{59}$$

all of which are subject to the interface conditions $[\mu_C] = 0$. The electrostatic potential, Ψ_e, is determined by the electroneutrality requirement inside the gel, namely,

$$(2c + n + h - c_l)\theta_s + z_m m_T = 0, \tag{60}$$

where z_m is the average charge per monomer. In this situation, where this charge depends on the amount of binding with ions,

$$z_m m_T = w - m. \tag{61}$$

Both the potential and polymer particle fraction are assumed to be zero outside the gel. Electroneutrality in the bath requires that

$$2c_b + n_b + h_b - c_{lb} = 0, \tag{62}$$

where the subscript "b" denotes the corresponding bath concentrations.

Several significant simplifications in the above equations result if we make the reasonable assumption that diffusion of ion species and their binding and unbinding reactions are fast compared to the swelling kinetics of the polymer network. Rapid diffusion implies that

$$\ln C + z_C\Psi_e = \text{constant}, \tag{63}$$

which because of the ion species interface condition (12),

$$C = C_b e^{-z_C\Psi_e}, \tag{64}$$

with $C = c$, n, h, c_l, $z_n = z_h = 1$, $z_c = 2$, and $z_{c_l} = -1$. The quantity Ψ_e at the interface is identified as the Donnan potential.

The assumption of fast chemistry implies (set the r.h.s. of Eqs. (51)–(54) and Eqs. (56)–(58) to zero) that

$$w = \frac{\theta_s}{K_c\phi_s^2}mc,\ v = \frac{\theta_s}{K_n\phi_s^2}mn,\ y = \frac{\theta_s}{K_h\phi_s^2}mh,\ x = \frac{\theta_s}{4K_c^2\phi_s^4}m^2c, \tag{65}$$

where $K_c = \frac{k_{-c}}{k_c}$, $K_n = \frac{k_{-n}}{k_n}$, $K_h = \frac{k_{-h}}{k_h}$, $K_x = \frac{k_{-x}}{k_x} = 4K_c$. It follows from Eqs. (50) and (65) that

$$\frac{\theta_p}{\nu_m N_A} = m\left(1 + \frac{\theta_s}{\phi_s^2}\frac{c}{K_c} + \frac{\theta_s}{\phi_s^2}\frac{n}{K_n} + \frac{\theta_s}{\phi_s^2}\frac{h}{K_h}\right) + m^2\frac{\theta_s}{2K_c^2\phi_s^4}c. \tag{66}$$

Taking Eq. (64) into account, this constraint becomes

$$\frac{\theta_p}{\nu_m N_A} = m\left(1 + \frac{c_b}{K_c}\frac{\theta_s}{\phi_s^2}e^{-2\Psi_e} + \left(\frac{n_b}{K_n} + \frac{h_b}{K_h}\right)\frac{\theta_s}{\phi_s^2}e^{-\Psi_e}\right) + m^2\frac{\theta_s}{2K_c^2\phi_s^4}c_b e^{-2\Psi_e}. \tag{67}$$

Under the assumption of fast diffusion and fast chemistry, the electroneutrality condition Eq. (60), reduces to

$$\theta_s(2c_b[e^{-2\Psi_e} - e^{\Psi_e}] + (n_b + h_b)[e^{-\Psi_e} - e^{\Psi_e}]) = -z_m m_T, \tag{68}$$

where

$$z_m m_T = -m\left(1 - \frac{\theta_s}{K_c\phi_s^2}c_b e^{-2\Psi_e}\right), \tag{69}$$

completing the description of the model.

In summary, the complete model consists of mass conservation equation (3), total volume conservation equation (4) together with force balance equations (6) and (7), and interface condition, Eq. (46), subject to the conditions Eq. (67) (monomer conservation) and Eq. (68) (electroneutrality). The crosslink fraction is $\alpha = \frac{2x}{m_T}$, and the van't Hoff factor is $\sigma_I = \nu_s \mathrm{N}_A \Sigma_I$, where

$$\Sigma_I^- = c_b(e^{-2\Psi_e} + 2e^{\Psi_e}) + (n_b + h_b)(e^{-\Psi_e} + e^{\Psi_e}), \tag{70}$$

and $\Sigma_I^+ = 3c_b + 2(n_b + h_b)$.

In summary, the assumptions made in the derivation of this model are

- Ionic species are dilute ($\phi_j \ll \phi_s$, $j \geq 3$) and do not contribute to the pressure ($\nu_j = 0, j \geq 3$).
- Ionic species are dissolved in the solvent.

- Crosslinking of polymer by divalent ions is transient, not permanent as with covalent bonds.
- Diffusion of ion species is fast and reaction of ionic species with monomer is fast compared to other kinetic processes.

III. EQUILIBRIUM ANALYSIS

We begin the study of these equations with an exploration of their equilibria. At equilibrium, there is no movement so that $\mathbf{v}_{p,s}(\mathbf{x}, t) = 0$, requiring θ_p to be uniform inside the gel. With no movement, the interface condition, Eq. (46), reduces to

$$\Sigma_{net} \equiv k_B T \left(\frac{M_p^-}{\nu_m} - \frac{M_s^-}{\nu_s} + \frac{T_0}{T}\frac{\mu_s^0}{\nu_s} + \frac{z_m}{\nu_m}\Psi_e + \frac{\sigma_I^-}{\nu_s} - \frac{\sigma_I^+}{\nu_s} \right) = 0. \tag{71}$$

Equilibrium solutions are the values (θ_p, Ψ_e, m) which satisfy Eqs. (67), (68), and (71).

The basic question that we wish to answer is how do the presence of polymer charges, divalent crosslinking, and dissolved ions affect the behavior of this gel. We address this question by examining the equilibrium solutions as functions of the bath concentrations, H_b, N_b, C_b, the dissociation constants, $K_{c,\,n,\,h}$, and the interaction parameters, $\epsilon_{1,\,2,\,3,\,4}$. (In what follows, we use non-dimensional concentrations and denote these with their corresponding capital letters, e.g., $N_b = \nu_s N_A n_b$, $M = \nu_m N_A m$, etc. as well as non-dimensional dissociation constants $K_{c,\,n,\,h}$.) To think about this it is useful to recognize that Σ_{net} defined in Eqs. (47) and (71) is the net swelling pressure and consists of three terms. Equilibrium is attained when these three terms are balanced.

The term $(\frac{M_p}{\nu_m} - \frac{M_s}{\nu_s} + \frac{T_0}{T}\frac{\mu_s^0}{\nu_s})$ represents the swelling pressure for an uncharged gel, including effects of divalent ion binding and crosslinking, and is closely related to the standard Flory-Huggins chemical potential.[27] The term $\frac{\sigma_I^-}{\nu_s} - \frac{\sigma_I^+}{\nu_s}$ represents osmotic swelling pressure coming from the difference between the concentrations of ions dissolved in the gel solvent and those dissolved in the bath, a term related to van't Hoff's law. The term $\frac{z_m \Psi_e}{\nu_m}$ represents swelling pressure coming from the fact that the monomers may be charged, i.e., the Donnan equilibrium. These latter terms are nonnegative, and increases in them promote swelling (i.e., a decrease in volume fraction). An important observation is that increasing $|z_m|$ or decreasing a bath concentration increases the swelling pressure, while the opposite changes decrease the swelling pressure. For example, in the case that there are only monovalent ions,

$$\begin{aligned} z_m \Psi_e &= z_m \ln\left(\frac{q + \sqrt{q^2+4}}{2}\right), \\ \sigma_I^- \sigma_I^+ &= (H_b + N_b)(\sqrt{q^2+4} - 2), \end{aligned} \tag{72}$$

where $q = \frac{z_m \theta_p}{(H_b + N_b)\theta_s}$, which are both increasing functions of $|z_m|$ and decreasing functions of $H_b + N_b$. Both of these swelling pressure terms are zero if $z_m = 0$, i.e., if there is no charge on the gel, or if $H_b + N_b \to \infty$.

The simplest case to consider is when there are no dissolved ions ($N_b = C_b = 0$), and there is no charge on the gel ($K_h = 0$). This problem has been thoroughly discussed in Ref. 28. For this, the equilibrium solutions are completely characterized by the interaction and standard free energy parameters,

$$\begin{aligned} i_0 &= z(\epsilon_1 + \epsilon_2) + 2\left(\frac{1}{N} - 1\right)\epsilon_1, \\ \mu_0^p &= -\epsilon_1 \frac{z}{2} + \epsilon_4\left(1 - \frac{1}{N}\right), \quad \mu_0^s = -\epsilon_2 \frac{z}{2}. \end{aligned} \tag{73}$$

As noted in Eq. (48), the function $k_B T(\frac{M_p}{\nu_m} - \frac{M_s}{\nu_s})$ is the derivative of the free energy per particle with respect to θ_p, and therefore zeros of this function correspond to extrema of the free energy. If $i_0 < 0$, the free energy has a unique minimum for all values of T, while if $i_0 > 0$ there is a range of temperature values for which the free energy is a double well potential, and for these temperatures there are three equilibria (two of which are stable, i.e., there is bistability).

For illustrative purposes, in the results that follow, the number of monomers per chain is fixed at $N = 3$, the coordination number at $z = 6$ and the temperature is set at $T = T_0$. It is known[28] that the qualitative behavior of the reduced system (with no charge, no crosslinking, and no dissolved ions) is not affected by changes of these parameters. Furthermore, for simplicity we take $\nu_m = \nu_s$, again with the recognition that the qualitative features of the system are not changed significantly if this is not the case. For the following discussion, we take $\epsilon_1 = -4.5$, $\epsilon_2 = -1.5$, $\epsilon_4 = 0$. For these values, the free energy is a single well potential and has a unique minimum. Thus, the fully simplified gel has no first order volume-transition behavior. However, as we describe below, the effects of charge and crosslinking can change this in significant ways.

A. Case 1: No dissolved ions

First, we explore the equilibrium states of the gel in an infinite water bath with no dissolved ions ($N_b = C_b = 0$). Hydrogen ions are available in the bath because of dissociation of water into hydrogen and hydronium, or because of the addition of HCl to the bath. H^+ ions can bind with the monomers with the binding reaction

$$M^- + H^+ \underset{k_{-h}}{\overset{k_h}{\rightleftharpoons}} MH. \tag{74}$$

Figure 2(a) shows the H_b-K_h phase diagram for the equilibrium states, with two regions, region A, in which there is a unique equilibrium solution and region B, in which there are three equilibria. The swelling curves (i.e., plots of equilibria vs. H_b) for four different values of the dissociation constant $K_h = \frac{k_{-h}}{k_h}$ are shown in Fig. 2(b). There are two qualitatively different types of swelling curves. If the gel is a strong acid ($\log_{10} K_h > -2.04$) there is gradual deswelling of the gel as the hydrogen bath concentration is increased, a second order/continuous volume transition. If the gel is a weak acid ($\log_{10} K_h < -2.04$), it can have three equilibrium states, depending on the bath concentration H_b, with hysteretic deswelling-swelling phase transition behavior. That is,

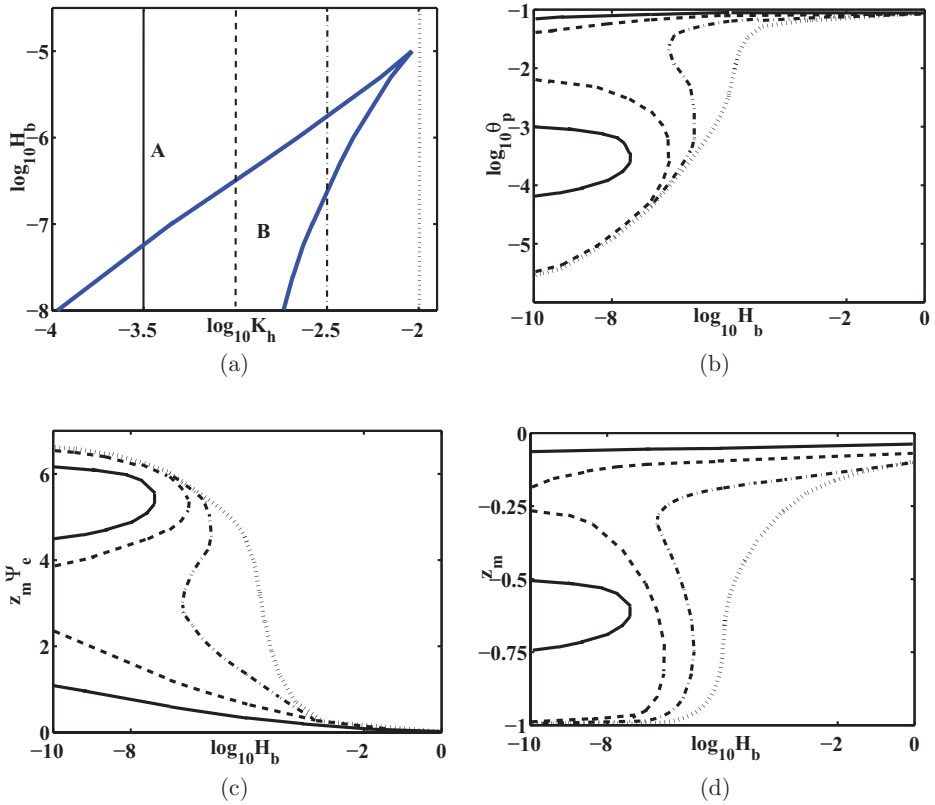

FIG. 2. (a) H_b-K_h phase diagram showing the regions with a unique equilibrium (region A) and three equilibria (region B). (b) Polymer volume fraction, θ_p, (c) average per particle Donnan potential, $z_m\Psi_e$, and (d) the average charge per monomer z_m, plotted vs. the (non-dimensional) hydrogen bath concentration H_b, for various dissociation constants, K_h, shown as vertical slices in (a). $\log_{10}K_h = -3.5$ (solid curve), $\log_{10}K_h = -3.0$ (dashed curve), $\log_{10}K_h = -2.5$ (dash-dotted curve), and $\log_{10}K_h = -2.0$ (dotted curve).

there is a discontinuous (first order) deswelling transition with increasing H_b and a discontinuous (first order) swelling transition with decreasing H_b.

With our choice of parameters, the uncharged gel has a unique equilibrium, so the appearance of a range of K_h for which the charged gel has three solutions is a surprise. However, further examination of parameter space reveals that this is a highly robust behavior. It results because the swelling pressure from the Donnan equilibrium is a positive function of θ_p with an interior maximum. As a result, ionization chemistry and the swelling pressures that result make the total free energy into a double well potential for certain parameter values, even though without ionization, it is a single well potential.

There is a very strong inverse relationship between the functions $\log_{10}\theta_p$ and $z_m\Psi_e$ that can be seen by comparing Figs. 2(b) and 2(c). That is, increasing $z_m\Psi_e$ correlates closely with decreasing $\log_{10}\theta_p$. This is easily understood since at low volume fraction the dominant contributions to the polymer chemical potential are from $\frac{1}{N}\ln\phi_p$, the Donnan potential, and the osmotic pressure. At equilibrium these must be in balance. For all parameter values examined here, the Donnan potential contribution to swelling pressure dominates that of the osmotic pressure. (In fact, the osmotic pressure difference due to the dissolved ions, $\sigma_I^- - \sigma_I^+$, is about two orders of magnitude smaller than the corresponding pressure due to the Donnan potential in the range of parameters considered here.) Hence, at low volume fractions $\frac{1}{N}\ln\phi_p$ and $z_m\Psi_e$ are roughly equal and opposite.

Notice, also, that the potential vanishes for sufficiently large hydrogen bath concentration. This is reasonable since, at large enough ion concentrations, all monomer binding sites are bound, eliminating the charge, and hence the potential. At high concentrations the gel is uncharged and deswollen.

In summary, the (physically relevant) solutions deswell as a function of increasing H_b. (The physically relevant solutions are the largest and smallest solutions, if there are three, because the intermediate solution is unstable.) This is because increasing hydrogen bath concentration leads to a decrease in ionization (Fig. 2(d)) and decreased swelling pressure (Fig. 2(c)), both contributing to deswelling.

B. Case 2: Dissolved monovalent ions

Next we consider the situation in which the gel is immersed in an infinite bath with fixed hydrogen concentration ($H_b = 10^{-7}$) containing monovalent cations, e.g., Na^+ (i.e., $C_b = 0$) with the binding reaction

$$M^- + Na^+ \underset{k_{-n}}{\overset{k_n}{\rightleftharpoons}} MNa, \tag{75}$$

in addition to that in Eq. (74). The phase diagrams for this case are readily determined from the phase diagram Fig. 2(a)

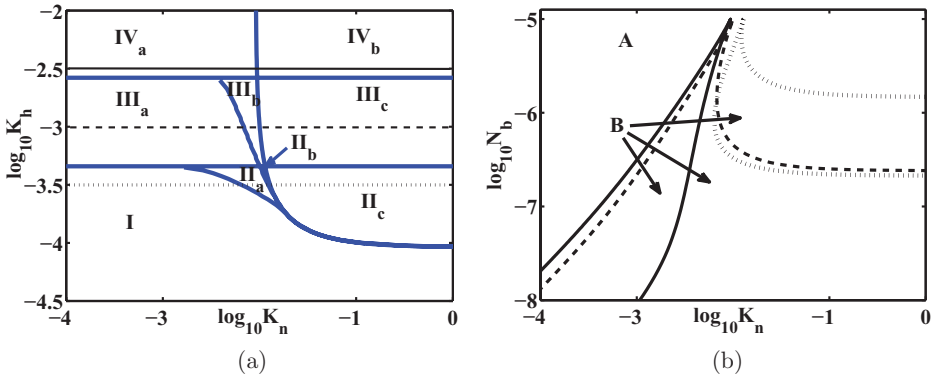

FIG. 3. (a) Sodium-hydrogen dissociation constant phase space, characterizing the sodium-hydrogen equilibrium phase space, (b) H_b-K_h phase diagrams showing the regions with a unique equilibrium (region A) and three equilibria (region B) for three different values of hydrogen dissociation constants. $\log_{10}K_h = -2.5$ (solid curve), $\log_{10}K_h = -3.0$ (dashed curve), and $\log_{10}K_h = -3.5$ (dotted curve).

for a single monovalent ion. This is because the equations, Eqs. (67), (68), and (71) depend on two parameters $p_h = H_b + N_b$ and $\frac{p_h}{p_K} = \frac{H_b}{K_h} + \frac{N_b}{K_n}$. Accordingly, a phase diagram in the N_b-K_n parameter plane can be found using this change of variables from the p_h-p_K phase diagram shown in Fig. 2(a). Figure 3(a) shows 9 different regions of K_h-K_n parameter space for which there are qualitatively different swelling curves, and Fig. 3(b) shows three of the five possible phase diagrams that result. Each phase diagram corresponds to a different horizontal slice of Fig. 3(a). Figures 4–6 show swelling curves (i.e., equilibria plotted vs. N_b) for several values of K_n.

For small K_h (weak acid, Region I in Fig. 3(a), swelling curve not shown), there is little change in the volume fraction as N_b is varied, because the gel is effectively uncharged with small Donnan potential or potential-induced osmotic pressure. There are no changes in volume fraction for an uncharged polymer as ion bath concentration changes, since there is no Donnan potential or osmotic pressure.

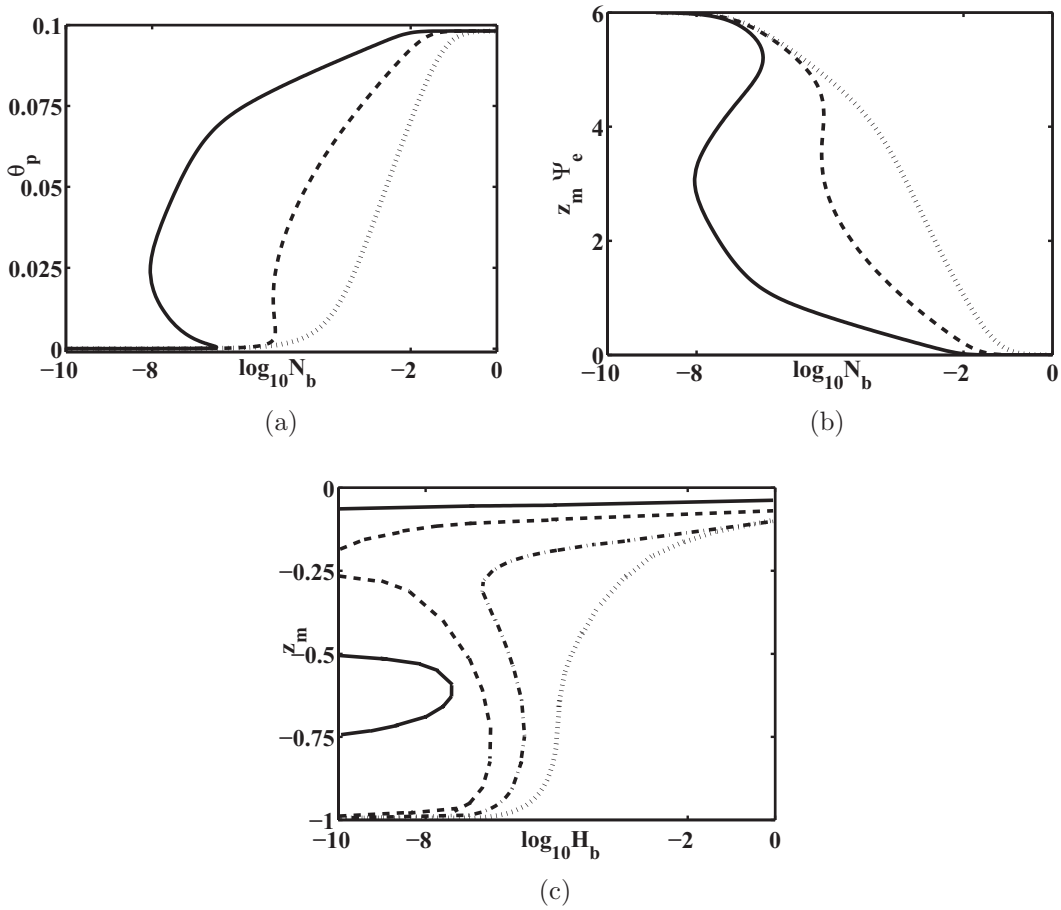

FIG. 4. (a) Polymer volume fraction, θ_p, (b) Donnan potential swelling pressure, $z_m\Psi_e$, and (c) average charge per monomer z_m, vs. non-dimensional Na^+ bath concentration N_b, for $\log_{10}K_h = -2.5$ and $\log_{10}K_n = -3.0$ (solid curve), $\log_{10}K_n = -2.0$ (dashed curve), and $\log_{10}K_n = -1.0$ (dotted curve).

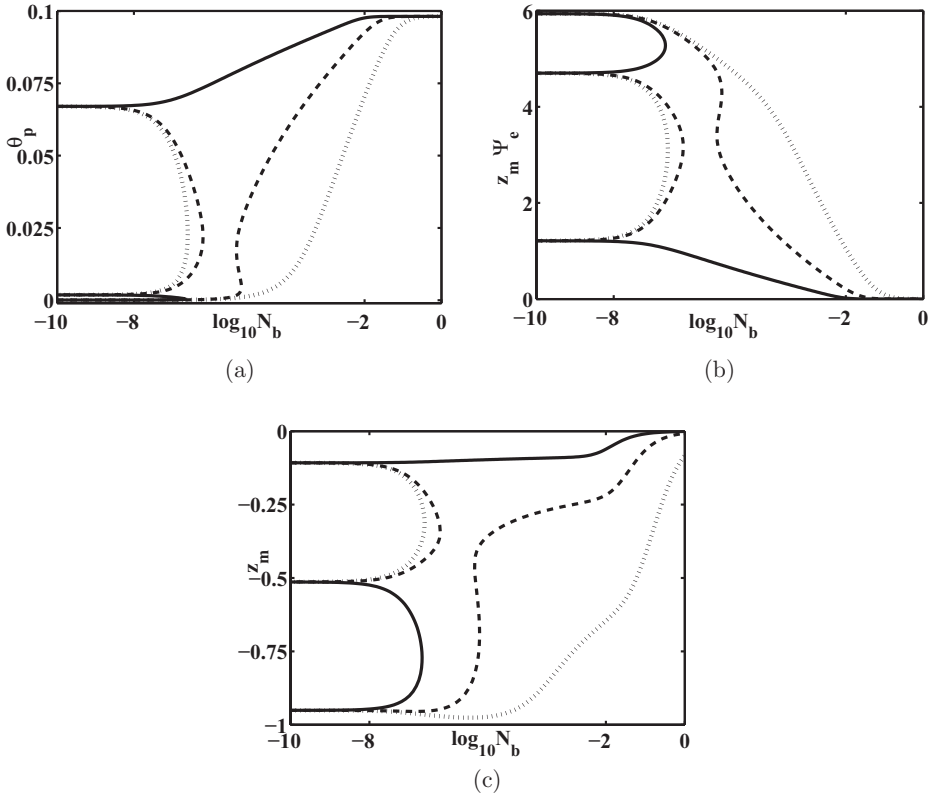

FIG. 5. (a) Polymer volume fraction, θ_p, (b) Donnan swelling pressure, $z_m\Psi_e$, and (c) average charge per monomer z_m vs. non-dimensional sodium bath concentration N_b, for hydrogen dissociation constant $\log_{10}K_h = -3.0$ and sodium dissociation constant $\log_{10}K_n = -3.0$ (solid curve), $\log_{10}K_n = -2.0$ (dashed curve), and $\log_{10}K_n = -1.0$ (dotted curve).

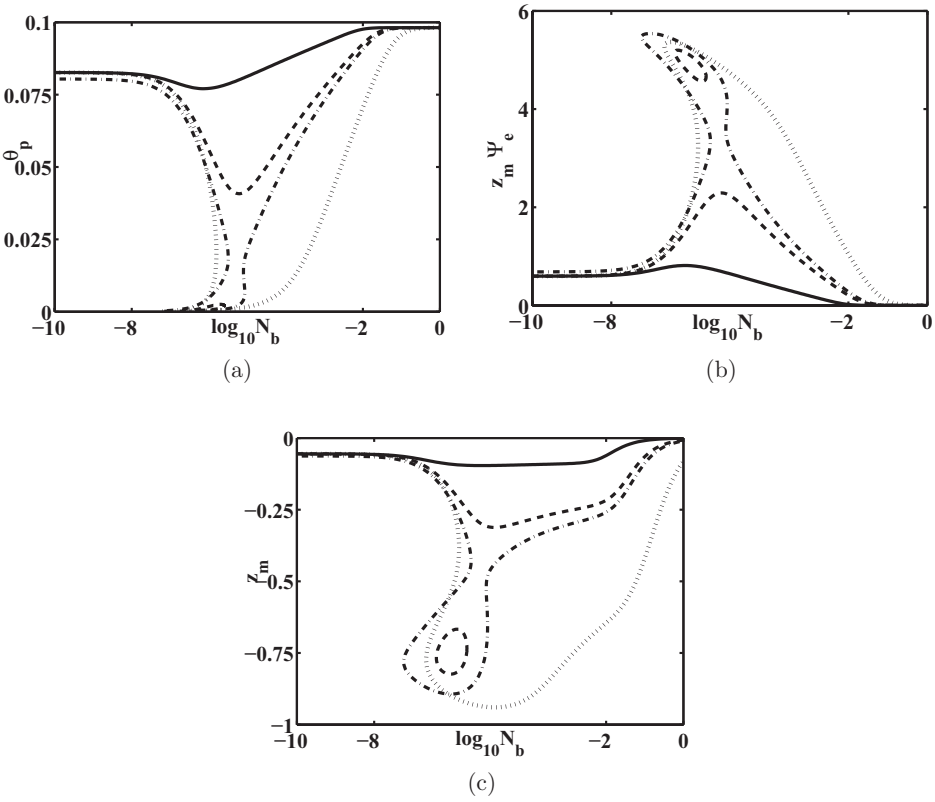

FIG. 6. (a) Polymer volume fraction, θ_p, (b) Donnan swelling pressure, $z_m\Psi_e$, and (c) average charge per monomer z_m vs. non-dimensional sodium bath concentration N_b, for hydrogen dissociation constant $\log_{10}K_h = -3.5$ and sodium dissociation constant $\log_{10}K_n = -3.0$ (solid curve), $\log_{10}K_n = -2.0$ (dashed curve), $\log_{10}K_n = -1.95$ (dash-dotted curve), and $\log_{10}K_n = -1.0$ (dotted curve).

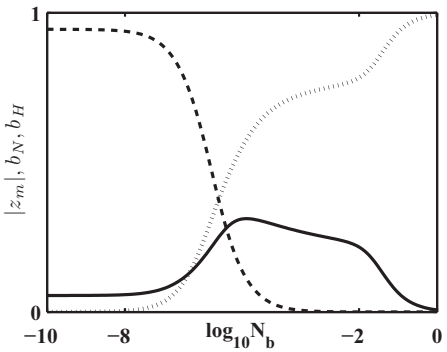

FIG. 7. Plots of total ionization $|z_m|$ (solid curve), hydrogen binding fraction b_H (dashed curve), and sodium binding fraction b_N (dotted curve) vs. N_b for hydrogen dissociation constant $\log_{10}K_h = -3.5$ and sodium dissociation constant $\log_{10}K_n = -2.0$.

For large K_h (strong acid, Regions IV$_{a,b}$ in Fig. 3(a)), there is swelling-deswelling behavior reminiscent of the single ion case seen in Fig. 2. These swelling curves θ_p vs. N_b are shown in Fig. 4(a), along with plots of the Donnan swelling pressure $z_m\Psi_e$ and the average monomer charge z_m in Figs. 4(b) and 4(c).

For intermediate values of K_h, with swelling curves shown in Figs. 5(a) and 6(a), there are additional swelling-deswelling features. In these regions, for small K_n (e.g. (solid curve)$\log_{10}K_n = -3.0$), the behavior is similar to that for the situation in Case 1 with small dissociation constant, i.e., slight deswelling as the bath concentration is increased. For larger K_n there is gradual deswelling ((dotted curve)$\log_{10}K_n = -1.0$) or a hysteretic deswelling-swelling phase transition ((dashed curve)$\log_{10}K_n = -2.0$ in Fig. 5) for sufficiently large N_b. However, for these curves there is a new feature, namely, a region with $N_b \approx 10^{-7}$ for which there is swelling, either gradual or through a phase transition, as the sodium bath concentration increases.

The explanation for these swelling features is that there is a complicated interplay between ionization (which promotes swelling) and increases in bath concentration which promote deswelling. This is illustrated in Fig. 7 where total ionization $|z_m|$, hydrogen binding fraction $b_H = \frac{y}{m_T} = \frac{[MH]}{m_T}$, and sodium binding fraction $b_N = \frac{v}{m_T} = \frac{[MNa]}{m_T}$ are plotted vs. N_b for the specific case in which $\log_{10}K_h = -3.5$ and $\log_{10}K_n = -2.0$ (see Fig. 6). In Fig. 7, we see that as N_b increases, there is an increase in sodium binding, and a decrease in hydrogen binding, with the net effect of an initial increase in the total ionization $|z_m|$, i.e., there is more unbinding of hydrogen than binding of sodium when the bath concentrations of the two ions are about the same. To understand this exchange better, notice that from Eqs. (64) and (65),

$$\frac{b_H}{b_N} = \frac{y}{v} = \frac{K_n}{K_h}\frac{H_b}{N_b}. \tag{76}$$

This implies that increases in N_b must be accompanied by increases in b_N and/or decreases in b_H. For the parameters in this figure $\frac{K_n}{K_h} = 31.6$, so that the ratio $\frac{b_H}{b_N}$ must decrease 31.6 times faster than the ratio $\frac{H_b}{N_b}$ as N_b increases. This forces significant unbinding of hydrogen, leading to the observed net ionization.

As noted before, ionization promotes swelling and increased ion bath concentration promotes deswelling; in this parameter range ionization swelling pressure dominates the ion bath concentration deswelling pressure. Thus, this ion exchange process explains the appearance of swelling regions in the swelling curves of Figs. 5 and 6.

C. Case 3: Dissolved divalent ions

Next, we consider a bath containing divalent Ca^{2+} ions. Unlike monovalent ions, the divalent Ca^{2+} ions can crosslink two monomers giving rise to the crosslinked species M_2Ca and the intermediate ions, MCa^+ (Eq. (1)). As before, we set the bath concentration of hydrogen to $H_b = 10^{-7}$. There are two cases to consider, first with $\epsilon_3 = 0$ and then with $\epsilon_3 < 0$ (see Eq. (34)).

With $\epsilon_3 = 0$, crosslinking has only a minor affect on the chemical potentials and so, not surprisingly, there is little difference from the monovalent ion case. The K_c-K_h parameter-space is again divided into nine different regions (Fig. 8(a)) for which there are qualitatively different swelling curves. Figure 8(b) shows three of the five possible phase diagrams that result. Each phase diagram corresponds to a different horizontal slice of Fig. 8(a). The swelling curves for these are not

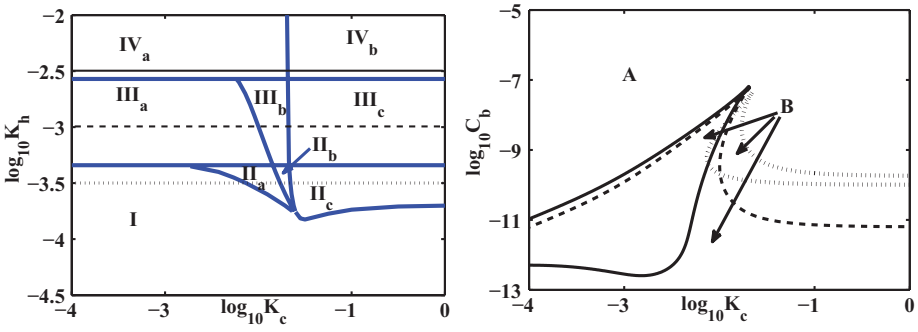

(a) (b)

FIG. 8. (a) Calcium-hydrogen dissociation constant phase space, characterizing the calcium-hydrogen equilibrium phase space: $\epsilon_1 = -4.5$, $\epsilon_2 = -1.5$, $\epsilon_3 = 0$; (b) C_b-K_c phase diagrams showing the regions with a unique equilibrium (region A) and three equilibria (region B) for three different values of hydrogen dissociation constants. $\log_{10}K_h = -2.5$ (solid curve), $\log_{10}K_h = -3.0$ (dashed curve), and $\log_{10}K_h = -3.5$ (dotted curve).

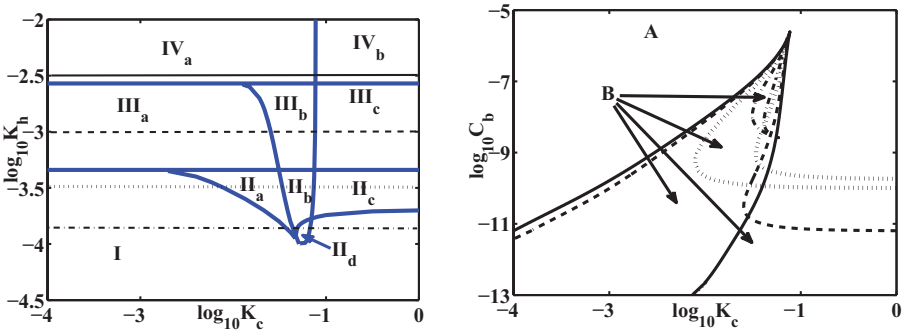

FIG. 9. (a) Calcium-hydrogen equilibrium phase space at $\epsilon_1 = -4.5$, $\epsilon_2 = -1.5$, and $\epsilon_3 = -26.667$. (b) C_b vs. K_c phase diagrams showing regions of a unique equilibrium (region A) and three equilibria (region B) at different hydrogen dissociation constants, $\log_{10}K_h = -2.5$ (solid curve), $\log_{10}K_h = -3.0$ (dashed curve), $\log_{10}K_h = -3.5$ (dotted curve), and $\log_{10}K_h = -3.8$ (dash-dotted curve).

shown, because they are qualitatively the same as those for the monovalent ion case.

Even with $\epsilon_3 = 0$, there are two differences between the monovalent and divalent cases that deserve mentioning. First, notice that the scale for C_b on the phase diagram Fig. 8(b) is much smaller than the scale for N_b in the phase diagram Fig. 3(b). This is because smaller amounts of calcium are needed to neutralize the charge of the monomer, since crosslinking involves two calcium-monomer binding reactions.

Second, in the monovalent case, binding always converts a negatively charged monomer into one without charge. In the divalent ion case, binding of a monomer with an ion converts it from a negatively charged ion into a positively charged ion. Thus, at sufficiently high calcium ion concentrations the average charge on the monomer is positive rather than negative. This has little effect on the overall swelling pressure since at high ion concentrations the charge on the gel is small relative to the overall number of available ions, and the Donnan and osmotic swelling pressures both vanish. As a consequence, at sufficiently high C_b the gel behaves as if it is uncharged.

When $\epsilon_3 < 0$, the K_c-K_h parameter-space is divided into the ten different regions shown in Fig. 9(a) for which there are qualitatively different swelling curves. Figure 9(b) shows four of the six possible phase diagrams that result. Each phase diagram corresponds to a different horizontal slice of Fig. 9(a).

The most significant effect of having $\epsilon_3 < 0$ is seen in the swelling curves. With $\epsilon_3 < 0$, crosslinked monomer-monomer interactions are energetically preferred to all other monomer-monomer interactions. Hence, crosslinking reduces the interaction energy and in that way promotes deswelling. This is most evident when the dissociation constant K_c is small, so that the monomer has a strong affinity for calcium, and when K_h is large, so that there are many binding sites available for crosslinking. We illustrate this effect with a series of plots in Fig. 10 comparing swelling curves for $\epsilon_3 = 0$ with those for $\epsilon_3 = -26.667$, all other parameters remaining the same. We also include a plot of α, the proportion of monomers that are crosslinked, vs. C_b.

The most apparent difference between the two sets of swelling curves is that for $\epsilon_3 < 0$, there is a region of C_b for which there is massive deswelling compared to the $\epsilon_3 = 0$ case (Fig. 10(a) vs. Fig. 10(b)). This is explained by the fact that crosslinking is energetically preferred, and more crosslinking is possible if the concentration of binding sites is higher, which in turn is facilitated if the gel is condensed.

There is another interesting feature of the $\epsilon_3 < 0$ swelling curves, namely, that for sufficiently high C_b, crosslinking is lost and the gel swells. This can be explained by the fact that at high calcium concentration, the species MCa^+ is dominant so that the gel is overall positively charged, and not crosslinked. Since crosslinking is lost, the effect of having $\epsilon_3 < 0$ is lost as well.

The equilibrium state of a gel is determined by the balance of three important forces, deswelling pressure from the ionic bath, swelling pressure from the ionization state, and deswelling pressure from the interaction energy preference that comes with divalent crosslinking (when $\epsilon_3 < 0$). Necessarily, changes in the equilibrium state are mediated by changes in this balance. To illustrate how this interplay works, in Fig. 11 are shown plots of the ionization state $|z_m|$, fractions of monomer bound to calcium $b_c = \frac{[MCa^+]}{m_T}$, and hydrogen b_H, vs. calcium ion bath concentration C_b with $\epsilon_3 = 0$ (a) and $\epsilon_3 = -26.667$ (b), and with dissociation constants $\log_{10}K_h = -3.5$ and $\log_{10}K_c = -3.0$ (corresponding to the dotted curves in Fig. 10). In Fig. 11(a), we see that as C_b increases, there is first an increase in ionization, caused by unbinding of hydrogen, followed by a decrease in ionization, caused by increased calcium crosslinking (seen in Fig. 10(c)), and then followed by increased ionization as crosslinks are exchanged for single calcium-monomer bonds, giving the monomer a net charge that approaches $z_m = 1$. Corresponding to these changes in ionization state, the gel (see Fig. 10(a)) first swells as hydrogen unbinds and then deswells as the calcium bath concentration becomes large.

For $\epsilon_3 < 0$, the balance of forces leads to a much different result. The ionization pattern seen in Fig. 11(b) is similar to that in Fig. 11(a), with ionization (unbinding of hydrogen) followed by de-ionization (mediated by calcium crosslinking), followed again by ionization as calcium crosslinks are replaced by single calcium-monomer bonds. However, the initial ionization swelling pressure is overwhelmed by the crosslinking energy gain and this leads to deswelling at small to intermediate C_b. For large C_b, where crosslinking is lost,

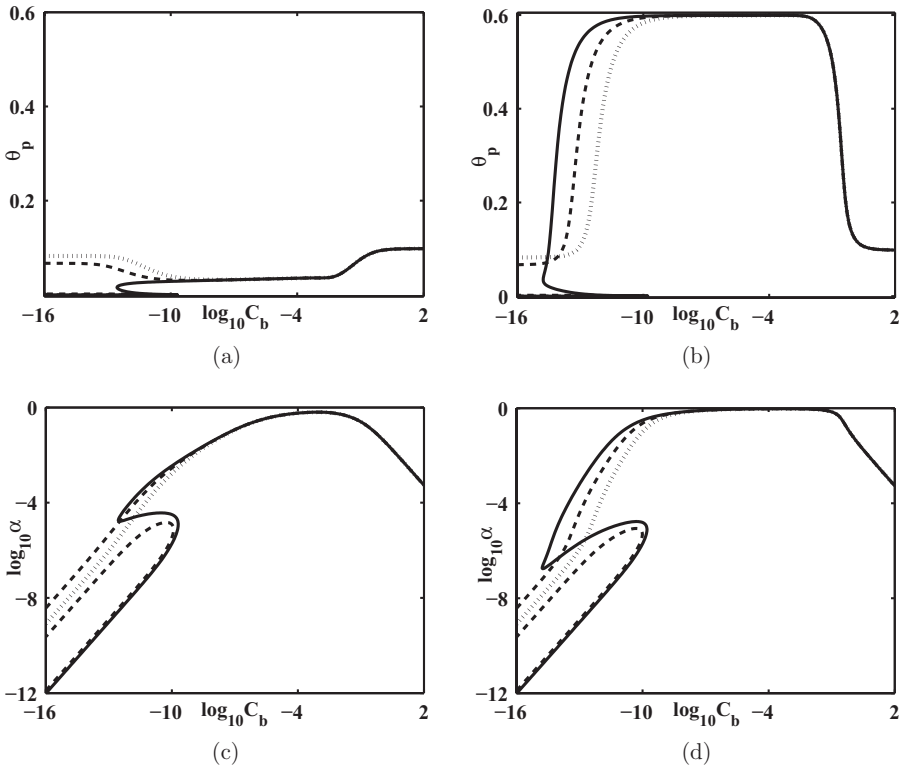

FIG. 10. (a) and (b) Polymer volume fraction θ_p, and (c) and (d) crosslink fraction α, vs. nondimensional calcium bath concentration C_b at calcium dissociation constant $\log_{10}K_c = -3.0$ and hydrogen dissociation constants $\log_{10}K_h = -2.5$ (solid curve), $\log_{10}K_h = -3.0$ (dashed curve), and $\log_{10}K_h = -3.5$ (dotted curve); (a) and (c) $\epsilon_3 = 0$ and (b) and (d) $\epsilon_3 = -26.667$.

swelling occurs because the effects of ionization are dominated by the effects of the ion bath concentration. In summary, we see large volume transitions when calcium crosslinking is energetically favored.

IV. DISCUSSION AND CONCLUSION

In this paper, we have given a systematic derivation and equilibrium analysis of a model to understand the swelling and deswelling of a mucin-like polyelectrolyte gel. We examine the effects of changes in the bath concentration of monovalent and divalent ions, changes in the ionization state of the gel because of binding/unbinding of ions, as well as changes in the divalent crosslinking. A feature that distinguishes mucin-like gels is that crosslinking is divalent hence transient, but not covalent, and so it is not appropriate to use rubber elasticity to model the gel's entropy.

Using this model, the equilibrium swelling phase diagrams were mapped out for the cases when the bath contained monovalent ions, e.g., Na^+, or divalent ions, e.g., Ca^{2+}. We learned that, generally speaking, increasing the bath concentration of the ion species leads to deswelling while increasing the ionization state leads to swelling, in agreement with experimental observations.[29] However, because of complex

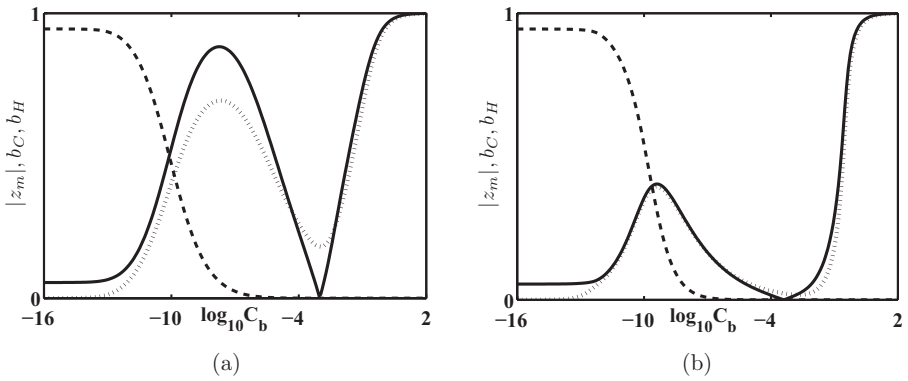

FIG. 11. Plots of total ionization $|z_m|$ (solid curve), hydrogen binding fraction b_H (dashed curve), and calcium binding fraction b_c (dotted curve), vs. C_b for $\log_{10}K_h = -3.5$ and $\log_{10}K_c = -3.0$, for $\epsilon_3 = 0$ (a) and $\epsilon_3 = -26.667$ (b).

interactions between competing forces, there can be hysteretic first order phase transitions of either type (i.e., deswelling with increases and swelling with decreases of bath concentrations, or the opposite). Furthermore, these hysteretic phase transition behaviors occur even though the free energy function of the deionized gel is a single well potential.

In addition, deswelling can be enhanced significantly if there is crosslinking with a divalent ion whose affinity for binding to monomers is sufficiently large, and if there is an energetic preference for the crosslinked monomer-monomer pair compared to the non-crosslinked monomer-monomer pair ($\epsilon_3 < 0$). The result is that there are dramatic deswelling or swelling transitions when divalent ion concentrations are changed. It is this dramatic deswelling/swelling behavior that sets mucin-like gels apart from other polyelectrolyte gels.

Because the swelling of a mucin-like gel following exocytosis is related to the exchange of monovalent and divalent ions and the associated changing of the crosslinking structure, the kinetics of this process is significantly different than that for a non-ionic polymer gel.[23] In this paper we focused on the derivation of the model and its equilibria. A full study of the kinetics of swelling will be the subject of a forthcoming article.

ACKNOWLEDGMENTS

This research was supported in part by National Science Foundation (NSF) Grant Nos. DMS-0540779, DMS-1122297, DMS-1160432, and National Institute of General Medical Sciences (NIGMS) Grant No. R01-GM090203.

APPENDIX: DERIVATION OF EQUATIONS OF MOTION

In this appendix, we give a derivation of Eqs. (6)–(8) and interface conditions (10) and (11), generalizing the derivation given in Ref. 23 to allow for multiple particles of differing sizes. We suppose that n_s is nonzero on the fixed domain Ω which is comprised of two subdomains, Ω_- and Ω_+, $\Omega = \Omega_- \cup \Omega_+$, and that n_m is nonzero on the subdomain Ω_-, and zero on Ω_+. Thus, n_s may have a jump discontinuity on the boundary Γ between Ω_- and Ω_+.

We wish to find the flow velocities that minimize the total rate of work. Accordingly, we seek to minimize the functional D_E specified in (5)

$$\begin{aligned} D_E = &\int_{\Omega_+} \left(\frac{1}{2}\theta_s \sigma_s(\mathbf{V}_s) : \dot{\varepsilon}(\mathbf{V}_s) - \frac{\mu_s}{\nu_s} \nabla \cdot (\theta_s \mathbf{V}_s) \right) dV \\ &+ \int_{\Omega_-} \left(\frac{1}{2}\theta_p \sigma_p(\mathbf{V}_p) : \dot{\varepsilon}(\mathbf{V}_p) + \frac{1}{2}\theta_s \sigma_s(\mathbf{V}_s) : \dot{\varepsilon}(\mathbf{V}_s) \right. \\ &+ \frac{1}{2}\xi \frac{n_m n_s}{n_m + n_s} (\mathbf{V}_p - \mathbf{V}_s)^2 \\ &\left. - \frac{\mu_p}{\nu_m} \nabla \cdot (\theta_p \mathbf{V}_p) - \frac{\mu_s}{\nu_s} \nabla \cdot (\theta_s \mathbf{V}_s) \right) dV \\ &+ \int_{\Omega} \sum_{j \geq 3} \left(\frac{1}{2}\xi_j \frac{n_j n_s}{n_j + n_s} (\mathbf{V}_s - \mathbf{V}_j)^2 - \mu_j \nabla \cdot (n_j \mathbf{V}_j) \right) dV, \end{aligned} \tag{A1}$$

over all admissible functions $(\mathbf{V}_j, P, \Psi_e)$, $j = 1, 2, \ldots, k$, where P and Ψ_e are Lagrange multipliers in the Gibb's free energy. Notice that $\theta_s = 1$, equivalently $n_m = 0$, on Ω_+. We specify the class of admissible flows as follows: For $\mathbf{V}_p$, we allow all smooth velocities on the interior of Ω_-, unspecified on the boundary Γ. For $\mathbf{V}_j, j > 1$, we allow all smooth velocities on the interiors of Ω_+ and Ω_-, with zero normal velocity on the boundary $\partial\Omega$, and with the fixed (but unknown) interface velocity $U = \frac{[n_j \mathbf{V}_j] \cdot \mathbf{n}}{[n_j]}$ on Γ. This latter condition is known as the Rankine-Hugoniot condition.

It is a subtle but important point that the class of admissible functions is not required to satisfy the incompressibility constraint. In fact, the beauty of Lagrange multipliers is that they relieve us of the requirement to vary only over the class of constrained functions. Thus, for admissible functions, the normal velocity of the edge of θ_p is not required to be the same as the normal velocity of the interface of θ_s, since requiring them to be the same is equivalent to requiring these velocities to satisfy the incompressibility constraint.

The Euler-Lagrange equations are calculated in the standard way: We let $\mathbf{V}_j = \mathbf{v}_j + \epsilon \delta \mathbf{v}_j$, where $\mathbf{v}_j, j = 1, 2, \ldots, k$, are the minimizers of D_E. Then, we require that the first variation, equivalently the derivative of D_E with respect to ϵ at $\epsilon = 0$, be zero. This implies that

$$\begin{aligned} 0 = &\int_{\Omega_+} \left(\theta_s \eta_s \, \dot{\varepsilon}(\mathbf{v}_s) : \nabla \delta \mathbf{v}_s + \theta_s \lambda_s (\nabla \cdot \mathbf{v}_s)(\nabla \cdot \delta \mathbf{v}_s) - \frac{\mu_s}{\nu_s} \nabla \cdot (\theta_s \delta \mathbf{v}_s) \right) dV \\ &+ \int_{\Omega_-} \left(\theta_s \eta_s \, \dot{\varepsilon}(\mathbf{v}_s) : \nabla \delta \mathbf{v}_s + \theta_s \lambda_s (\nabla \cdot \mathbf{v}_s)(\nabla \cdot \delta \mathbf{v}_s) - \xi \frac{n_m n_s}{n_m + n_s} (\mathbf{v}_p - \mathbf{v}_s) \delta \mathbf{v}_s - \frac{\mu_s}{\nu_s} \nabla \cdot (\theta_s \delta \mathbf{v}_s) \right) dV \\ &+ \int_{\Omega_-} \left(\theta_p \eta_p \, \dot{\varepsilon}(\mathbf{v}_p) : \nabla \delta \mathbf{v}_p + \theta_p \lambda_p (\nabla \cdot \mathbf{v}_p)(\nabla \cdot \delta \mathbf{v}_p) + \xi \frac{n_m n_s}{n_m + n_s} (\mathbf{v}_p - \mathbf{v}_s) \delta \mathbf{v}_p - \frac{\mu_p}{\nu_m} \nabla \cdot (\theta_p \delta \mathbf{v}_p) \right) dV \\ &+ \int_{\Omega} \sum_{j \geq 3} \left(\xi_j \frac{n_j n_s}{n_j + n_s} (\mathbf{v}_j - \mathbf{v_s}) \delta \mathbf{v}_j - \mu_j \nabla \cdot (n_j \delta \mathbf{v}_j) \right) dV \\ &+ \int_{\Omega} \sum_{j \geq 3} \left(\xi_j \frac{n_j n_s}{n_j + n_s} (\mathbf{v}_s - \mathbf{v}_j) \delta \mathbf{v}_s \right) dV. \end{aligned} \tag{A2}$$

Now, apply the divergence theorem to find

$$\begin{aligned}0 = &\int_{\Omega_+}\left(-\nabla\cdot(\theta_s\sigma_s(\mathbf{v}_s))+\frac{\theta_s}{\nu_s}\nabla\mu_s\right)\delta\mathbf{v}_s dV\\ &+\int_{\Omega_-}\left(-\nabla\cdot(\theta_s\sigma_s(\mathbf{v}_s))-\xi\frac{n_m n_s}{n_m+n_s}(\mathbf{v}_p-\mathbf{v}_s)+\frac{\theta_s}{\nu_s}\nabla\mu_s\right)\delta\mathbf{v}_s dV\\ &\int_{\Omega_-}\left(-\nabla\cdot(\theta_p\sigma_p(\mathbf{v}_p))+\xi\frac{n_m n_s}{n_m+n_s}(\mathbf{v}_p-\mathbf{v}_s)+\frac{\theta_p}{\nu_m}\nabla\mu_p\right)\delta\mathbf{v}_p dV\\ &+\int_{\Omega}\sum_{j\geq 3}\left(\xi_j\frac{n_j n_s}{n_j+n_s}(\mathbf{v}_j-\mathbf{v}_s)+n_j\nabla\mu_j\right)\delta\mathbf{v}_j dV\\ &+\int_{\Omega}\sum_{j\geq 3}\left(\xi_j\frac{n_j n_s}{n_j+n_s}(\mathbf{v}_s-\mathbf{v}_j)\delta\mathbf{v}_s\right)dV\\ &+\int_{\Gamma}\left(\theta_p\mathbf{e}_p\delta\mathbf{v}_p+[\theta_s\mathbf{e}_s\delta\mathbf{v}_s]-\sum_{j\geq 3}[n_j\mu_j\delta\mathbf{v}_j]\right)\cdot\mathbf{n}dS,\end{aligned}\tag{A3}$$

where $\mathbf{e}_p=\sigma_p(\mathbf{v}_p)\cdot\mathbf{n}-\frac{\mu_p}{\nu_m}\mathbf{n}$, $\mathbf{e}_s=\sigma_s(\mathbf{v}_s)\cdot\mathbf{n}-\frac{\mu_s}{\nu_s}\mathbf{n}$, $\mathbf{n}$ is the outward unit normal vector at the interface Γ, and by $[g]$, we mean the jump in the quantity g across the interface Γ.

Treating $\boldsymbol{\delta}\mathbf{v}_p$, $\boldsymbol{\delta}\mathbf{v}_s$, and $\boldsymbol{\delta}\mathbf{v}_j$, $j\geq 3$ on the interior of Ω_- as independent and arbitrary, we find the force balance equations:

$$-\nabla\cdot(\theta_p\sigma_p(\mathbf{v}_p))+\xi\frac{n_m n_s}{n_m+n_s}(\mathbf{v}_p-\mathbf{v}_s)+\frac{\theta_p}{\nu_m}\nabla\mu_p=0,\tag{A4}$$

$$\begin{aligned}&-\nabla\cdot(\theta_s\sigma_s(\mathbf{v}_s))-\xi\frac{n_m n_s}{n_m+n_s}(\mathbf{v}_p-\mathbf{v}_s)\\ &+\sum_{j\geq 3}\xi_j\frac{n_j n_s}{n_j+n_s}(\mathbf{v}_s-\mathbf{v}_j)+\frac{\theta_s}{\nu_s}\nabla\mu_s=0,\end{aligned}\tag{A5}$$

$$\xi_j\frac{n_j n_s}{n_j+n_s}(\mathbf{v}_j-\mathbf{v}_s)+n_j\nabla\mu_j=0.\tag{A6}$$

On the interior Ω_+, where $\theta_s=1$ and $\nabla\mu_s=\nu_s\nabla P$, we obtain Stokes' equation:

$$-\nabla\cdot\sigma_s(\mathbf{v}_s)+\nabla P=0.\tag{A7}$$

Requiring the variation of D_E with respect to P to vanish yields the conservation equation:

$$\nabla\cdot(\theta_p\mathbf{v}_p+\theta_s\mathbf{v}_s)=0,\tag{A8}$$

on the interior of Ω_- and $\nabla\cdot\mathbf{v}_s=0$ on the interior of Ω_+. Finally, requiring the variation of D_E with respect to Ψ_e to vanish yields the electroneutrality condition equation (60) on the interior of Ω_+ and (62) on the interior of Ω_-. An important feature of these force balance equations is that they satisfy Newton's third law. In particular, the sum of all drag forces is zero, as is the sum of all chemical potential-derived forces, owing to the readily verified fact that

$$\sum_j n_j\nabla\mu_j=0.\tag{A9}$$

On the interface, because $\delta\mathbf{v}_p$ is arbitrary, it must be that

$$\mathbf{e}_p\cdot\mathbf{n}=0,\tag{A10}$$

while the interface condition for $\mathbf{v}_s$ implies that $[\theta_s\delta\mathbf{v}_s]\cdot\mathbf{n}=0$, so that

$$(\mathbf{e}_p^+-\mathbf{e}_p^-)\cdot\mathbf{n}=0.\tag{A11}$$

Using the definitions of $\mathbf{e}_p$ and $\mathbf{e}_s$, we find the interface conditions (10) and (11).[30]

Similarly, for the ion species, the condition $[n_j\delta\mathbf{v}_j]\cdot\mathbf{n}=0$ implies that

$$\mu_j^+=\mu_j^-.\tag{A12}$$

[1] P. Verdugo, Adv. Polym. Sci. **110**, 145–156 (1993).
[2] P. Verdugo, I. Deyrup-Olsen, A. W. Martin, and D. L. Luchtel, *Mechanics of Swelling*, NATO ASI Series Vol. H 64, edited by T. K. Karalis (Springer-Verlag, 1992), pp. 671–681.
[3] J. Barasch, B. Kiss, A. Prince, L. Saiman, D. Gruenert, and Q. Awqati, Lett. Nature **352**, 70–74 (1991).
[4] P. W. Cheng, T. F. Boat, K. Cranfill, J. R. Yankaskas, and R. Boucher, J. Clin. Invest. **84**, 68–72 (1989).
[5] R. Kuver, J. H. Klinkspoor, W. R. A. Osborne, and S. P. Lee, Glycobiology **10**, 149–157 (2000).
[6] J. P. Vilar, Am. J. Respir. Cell Mol. Biol. **36**, 183–190 (2007).
[7] R. Bansil and B. S. Turner, Curr. Opin. Colloid and Interface Sci. **11**, 164–170 (2006).
[8] P. Verdugo, Chap. 19 in *Cilia, Mucus, and Mucociliary Interactions* (Marcel Decker, New York, 1998), pp. 167–189.
[9] P. Verdugo, M. Aitken, L. Langley, and M. Villalon, Biorheology **24**, 625–633 (1987).
[10] J. Cohen and Z. Priel, Macromolecules **22**, 2356 (1989).

[11]F. Horkay, P. J. Basser, A.-M. Hecht, and E. Geissler, Macromolecules **45**, 2882 (2012).
[12]F. Horkay, P. J. Basser, D. J. Londono, A.-M. Hecht, and E. Geissler, J. Chem. Phys. **131**, 184902 (2009).
[13]D.-W. Yin, F. Horkay, J. F. Douglas, and J. J. de Pablo, J. Chem. Phys. **129**, 154902 (2008).
[14]Y. Zhang, J. F. Douglas, B. D. Ermi, and E. J. Amis, J. Chem. Phys. **114**, 3299 (2001).
[15]T. Tanaka, D. Filmore, S. T. Sun, I. Nishio, G. Swislow, and A. Saha, Phys. Rev. Lett. **45**, 1636 (1980).
[16]A. E. English, S. Mafe, J. Manzanares, X. Yu, A. Y. Grosberg, and T. Tanaka, J. Chem. Phys. **104**, 8713–8720 (1996).
[17]C. Wolgemuth, A. Mogilner, and G. Oster, Eur. Biophys. J. **33**, 146–158 (2004).
[18]S. K. De, N. R. Aluru, B. Johnson, W. C. Crone, D. J. Beebe, and J. Moore, J. Microelectromech. Syst. **11**, 544–555 (2002).
[19]E. Kokufuta, Langmuir **21**, 10004–10015 (2005).
[20]O. V. Zribi, H. Kyung, R. Golestanian, T. B. Liverpool, and G. C. L. Wong, Phys. Rev. E **73**, 031911 (2006).
[21]S. Hirotsu, J. Chem. Phys. **94**, 3949–3957 (1990).
[22]M. Doi, J. Phys. Condens. Matter **23**, 284118 (2011).
[23]J. P. Keener, S. Sircar, and A. L. Fogelson, SIAM J. Appl. Math. **71**, 854–875 (2011).
[24]C. W. Wolgemuth, Biophys. J. **95**, 1564–1574 (2008).
[25]M. Doi, *Introduction to Polymer Dynamics* (Oxford University Press, Oxford, England, 1996).
[26]P. J. Flory, *Principles of Polymer Chemistry* (Cornell University Press, Ithaca, NY, 1953).
[27]P. J. Flory, Proc. R. Soc. Lond., Ser. A. **351**, 351–380 (1976).
[28]J. P. Keener, S. Sircar, and A. Fogelson, Phys. Rev. E **83**, 041802 (2011).
[29]S. Hirotsu, Y. Hirokawa, and T. Tanaka, J. Chem. Phys. **87**, 1392–1395 (1987).
[30]This corrects the interface conditions used in Ref. 23.